Fluid viscoelasticity drives self-assembly of particle trains in a straight microfluidic channel

Francesco Del Giudice*
Systems and Process Engineering Centre, College of Engineering, Swansea University, Fabian Way, Swansea SA1 8EN, UK

Gaetano D'Avino, Francesco Greco, and Pier Luca Maffettone
Dipartimento di Ingegneria Chimica, dei Materiali e della Produzione Industriale, Universitá degli Studi di Napoli Federico II, Piazzale Tecchio 80, 80125, Naples, Italy.

Amy Q. Shen
Micro/Bio/Nanofluidics Unit, Okinawa Institute of Science and Technology Graduate University, 1919-1 Tancha, Onna-son, Kunigami-gun, Okinawa, 904-0495, Japan

Strings of equally-spaced particles (particle train) are tremendously important in a variety of microfluidic applications. By using inertial microfluidics, particle trains can be formed near the channel walls. However, the high particle rotation and large local shear gradient near the microchannel walls can lead to blurred images and cell damage, thus negatively affecting applications related to flow cytometry. To address this challenge, we demonstrate that adding a tiny amount of hyaluronic acid biopolymer to an aqueous suspension drives self-assembly a particle train on the centreline of a square-shaped straight microchannel, with a throughput up to ∼2400 particles/s. The fraction of equally spaced particles increases by increasing the volumetric flow rate and the distance from the channel inlet. Numerical simulations corroborate the experimental observations and, together with a simple qualitative argument on the particle train stability, shed insights on the underlying mechanism leading to particle ordering.

INTRODUCTION

Controlling the spacing between particles and cells at micron size level, hereafter particle or cell *ordering*, dramatically impacts on a variety of applications ranging from biomedical engineering to material science. Particle and cell ordering is essential in applications such as flow cytometry [1–3], cell separation [4] particle encapsulations, [5, 6], and microfluidic particle or droplet crystals [7–9]. In material science, optical and acoustic properties of metamaterials can be tuned by the spatial composition of particles [10, 11]. In tissue engineering, the local arrangement of cells (cell *architecture*) is a crucial parameter for the design of 3D scaffolds [12] or printed tissues [13].

Particle *trains* (strings of ordered particles) organised on multiple streamlines were first observed by Segré and Silberberg [14], by using the inertial focusing principle. In their work, they employed particles with diameters in the range of $0.32 < d < 1.7$ mm suspended in a 1,3-butanediol and water mixture. They argued that the train formation was due to particle-particle hydrodynamic interactions. Matas *et al.* [15] observed trains of 425 μm and 825 μm particles organised on multiple streamlines of a tube with 8 mm diameter. They ascribed the formation of trains to the coupling of particle-particle hydrodynamic interactions and inertial forces, as also theoretically proposed later by Lee *et al.* [7]. Di Carlo *et al.* [16] achieved particle trains on multiple streamlines in a square-shaped microchannel with a height of 50 μm. In their work, they employed particles with diameter in the range of $4 < d < 20$ μm suspended in water, at a concentration range of $0.1 < \phi < 1$ vol%. Single-line particle and cell trains have been obtained by employing inertial microfluidic in a curved 50 μm channel [1] and in a straight channel with multiple non-rectangular cross-sections [17]. However, in both cases, particle/cell trains were observed near the channel walls where the particle/cell rotation and the local shear gradient are large. Large particle/cell rotation may lead to blurred images in cytometry applications that use line-scan-based interrogation, as reported by Goda *et al.* [18]. In addition, high local shear gradients may result in damaging delicate cells. Hence, particle trains should develop on the channel centreline, where both particle/cell rotation and local shear gradient are minimal.

Recently, the addition of polymer to aqueous suspensions was found to promote transversal migration of suspended particles towards the centreline of a straight microchannel [19–21], due to internal *viscoelastic* forces [22]. However, the majority of existing studies [23–25] dealing with particles in viscoelastic fluids flowing in microchannels have only considered very dilute suspensions (volume particle concentration lower than 0.1%). Hence, particles essentially behave as isolated objects and, upon alignment, the interparticle distances are so large that particle-particle hydrodynamic interactions could be considered negligible. To the best of our knowledge, only few works examined flow of suspension at higher particle concentrations. Xiang *et al.* [26, 27] found that particles suspended in a near constant-viscosity liquid at $\phi = 0.5$ vol% were focused on a single streamline in a

* Corresponding Author: francesco.delgiudice@swansea.ac.uk

curved 50 μm square-shaped microchannel, but did not display any ordered structure. For a similar suspending liquid, Kang *et al.* [28] found that particles with $5 < \phi < 10$ vol% segregated around the centreline of a straight 50 μm microchannel without forming particle trains. D'Avino *et al.* [29] employed numerical simulations to study the effect of viscoelasticity-mediated particle-particle hydrodynamic interactions on the spacing between pairs and triplets of particles suspended in a viscoelastic liquid with shear-thinning properties, at the centreline of a pressure-driven channel flow. They found that, in strongly shear-thinning elastic fluids, the distances between three aligned particles increase up to a value such that the particles behave like isolated objects. In case of a multi-particle system, such repulsion dynamics might potentially lead to equally-spaced structures. However, the limitation to only three particles remains, thus it is still uncertain whether particle trains can be effectively achieved. So far, neither experimental nor numerical evidence of particle trains in viscoelastic liquids has been reported. It should also be emphasised that shear-thinning liquids have always been considered as detrimental for particle alignment, since particles tend to migrate towards the channel walls [30, 31]. Only very recently, Del Giudice *et al.* [32] showed that moving particles can be aligned on the centreline of a straight square-shaped microchannel, even in a shear-thinning liquid, by increasing the ratio of the particle size to the channel height. Therefore, further investigation on viscoelastic particle ordering seems at order.

In this work, we demonstrate that simple addition of 1 wt% hyaluronic acid biopolymer to an aqueous suspension drives self-assembly of single-line particle trains on the centreline of a squared-shaped straight microchannel. Particles with diameter $d = 20$ μm first align, and then self-order on the centreline of the glass microchannel, with channel height $H = 100$ μm, and with a throughput up to ~ 2400 particles/s. Our results show that shear-thinning of the suspending liquid is in fact advantageous to achieve viscoelastic particle ordering. Numerical simulations corroborate the experimental observations and, together with a simple qualitative argument on the particle train stability, shed insights on the underlying mechanism leading to particle ordering.

METHODS

Preparation and characterization of the suspensions

We employed two solutions of hyaluronic acid HA (Molecular weight $M_w = 900$ kDa, Sigma Aldrich) at mass concentrations of 1 wt% and 0.1 wt% in phosphate buffer saline (PBS, Sigma Aldrich, Japan). HA 1 wt% was prepared by adding polymer powder to MilliQ water at room temperature, and the solution was shook vigorously to allow dissolution of polymer. HA 0.1 wt% was prepared by diluting ten times the HA 1 wt% solution with PBS. Glycerol at 25 wt% (Nacalai, Japan) was subsequently added to HA 0.1 % to prevent particle sedimentation. Glycerol was not needed for the premixed HA 1 wt%, due to the high viscosity of the fluid. Polystyrene particles (Polysciences Inc.) of 20 μm in diameter were added to both polymer solutions at volume concentrations $\phi = 0.3\%$, $\phi = 0.6\%$, and $\phi = 1\%$. The addition of particle to HA 1 wt% requires multiple steps of mixing due to the high viscosity of the solvent. No surfactant was used to enhance dispersion. Both suspensions were filtered by a standard 40 μm filter to remove potential aggregates.

Rheological measurements were carried out on a stress controlled rheometer (Anton Paar MCR 502) with a stainless steel cone and plate geometry (50 mm of diameter, 1° angle). Solvent trap was used to avoid fluid evaporation. Temperature was kept constant at $T = 22°$C.

Microfluidic device

The inlet to the glass channel was fabricated of polymethylmethacrylate (PMMA, substrate thickness 1 mm, Kuraray Co. Japan), using a micromilling machine [33] (Minitech CNC Mini-Mill). Fabrication was carried out using 300 μm and 200 μm tips. Channel depth was kept constant to 200 μm. Finally, a hole was made to allow pumping of the suspension. The inlet to the glass channel was bonded on another PMMA substrate by immersing the two pieces in absolute ethanol (Sigma-Aldrich) for 20 minutes. The two PMMA pieces were then put on a hot press (Imoto IMC-180C, Japan) with plate temperature $T = 40°$ and pressure $\Delta P = 0.4$ MPa for 20 minutes (ΔP is the difference between the final pressure and the pressure detected when the hot plates touched the two PMMA pieces). Square-shaped glass microchannel (Vitrocom) with internal height $H = 100$ μm and external height of 200 μm was glued directly to the PMMA inlet.

Experimental procedure

The fluid was pumped at several volumetric flow rate Q using a high precision Harvard PHD-Ultra syringe pump. We used Hamilton gas tight glass syringes to avoid wall deformation from affecting the rate of fluid delivery into the microchannel.

First, we imposed $Q = 10$ μl/min for 10 minutes to allow flow stabilization. After flow stabilization, images were recorded using an high speed camera (Phantom Miro M310, Vision Research). Since HA is expensive, images at higher Q were acquired as follows. The flow rate was kept to $Q = 10$ μl/min for 10 minutes, and then the higher flow rate was imposed. After 30 seconds, images were recorded, and the flow was subsequently reset to $Q = 10$ μl/min. This procedure was not expected to bias our analysis. Indeed, the volume of the whole glass channel is $H \times H \times L = 0.1 \times 0.1 \times 100 = 1$ mm$^3 = 1\mu$l. For $Q = 20$ μl/min, $Q = 50$ μl/min, and $Q = 100$ μl/min the volume of fluid flowed through the channel after 30 s

was 10 μl, 50 μl, and 100 μl, respectively, always higher than 1 μl. Therefore, during image acquisition, the sample was always fresh.

Determination of the distance between the particles

Particles from 1500 acquired images were tracked using a freely available particle tracking subroutine for IDL (Harris Geospatial Solution) [34]. Notice that when two particles were in contact, the subroutine was unable to distinguish between the two particles, thus it has been treated as a single one. Bigger aggregates, instead, have been disregarded from the analysis. The spacing between particles Δz was evaluated by using an homemade subroutine for Mathematica (Wolfram), and then normalized by the particle diameter d. Histograms were then evaluated using Origin Pro 2017, with binning size equal to d. The two boundary ends were set to 0 and $30d$.

RESULTS AND DISCUSSION

Experiments

Particle ordering in a straight microchannel was studied experimentally by suspending 20 μm polystyrene particles in a PBS solution containing 1 wt% hyaluronic acid (HA), at three particle loadings, $\phi = 0.3$ vol%, $\phi = 0.6$ vol%, and $\phi = 1$ vol%. To avoid particle clogging, we designed a multi-contraction inlet made of polymethylmethacrylate (gray device in Figure 1a). The square-shaped glass microchannel with internal height $H = 100$ μm and total length $L = 10$ cm was glued inside the multi-contraction inlet. Glass channel is preferred over the most commonly used polydimethylsiloxane (PDMS) since it is more rigid and therefore prevents channel deformation at high flow rates (channel deformation can affect transversal migration of particles [36]).

Results from different experimental conditions were quantified through the Deborah number De, which is the ratio between the characteristic time λ of the fluid and the characteristic time t_f of the flow. The Deborah number can also be regarded to as a characteristic ratio between elastic and viscous forces in flow conditions; whichever interpretation is adopted, the Newtonian liquid corresponds to $De = 0$ whereas $De > 0$ implies a certain degree of elasticity of the fluid. For a channel with a square cross section, the Deborah number is defined as:

$$De = \frac{\lambda}{t_f} = \frac{\lambda Q}{H^3}, \tag{1}$$

where Q is the volumetric flow rate. In our experiments, the range of Deborah number investigated is $6.2 < De < 62$, corresponding to the volumetric flow rate of $10 < Q < 100$ μl/min.

Hyaluronic acid 1 wt% in PBS drives formation of particle trains

Previous works highlighted that the rheology of the suspending liquid would affect the focusing dynamics of the flowing particles [23, 24, 37]. HA 1 wt% in PBS displays an almost constant shear viscosity η up to a shear rate of $\dot{\gamma} \sim 10$ s^{-1}, followed by a *shear-thinning* behavior (shear viscosity η decreases with increasing the shear rate) as $\dot{\gamma}$ increases (Figure 1b). The elasticity of the solution was quantified through the longest relaxation time λ, evaluated from the measurement of the storage modulus G' and the loss modulus G'' (inset of Figure 1b). Following a standard rheological procedure (i.e., small angle oscillatory shear) [35], we obtained $\lambda = 37$ ms from the intersection of the dashed and the dashed-dotted lines fitting the data at low frequencies. In summary, PBS solution containing 1 wt% HA exhibits flow dependent shear viscosity η and elastic properties quantified by $\lambda = 37$ ms.

The experiments were first performed for a suspension at a particle concentration $\phi = 0.6$ vol% in PBS containing 1 wt% HA. At a fixed distance from the inlet $L_\mathrm{z}/H = 800$ ($L_\mathrm{z} = 8$ cm), around 18 particles were visible within the observed portion of the channel $L_\mathrm{obs} = 60d = 1.2$ mm (left panel of Figure 1c). As the Deborah number was increased, an increasing fraction of particles became progressively equally spaced, i.e., *ordered*. From a simple geometrical argument (see Eq. 2 below), 18 particles along L_obs, if ordered, should be spaced with a distance between their centers $s_{theo} = L_\mathrm{obs}/18 \sim 3.3d$ (in dimensionless terms, $s^*_{theo} = s_{theo}/d = 3.3$). We indeed observed a dominant peak in the histograms at a dimensionless distance $s^* = 3.5$, in good agreement with the geometrical value. The peak of the distance distribution at $s^* = 3.5$ was also found to be independent of the Deborah number (Figure 1c). Interestingly, the fraction f of ordered particles with $s^* = 3.5$ was found to double from $f \sim 0.2$ at $De = 6.2$ ($\dot{\gamma} \simeq 170$ s^{-1}) to $f \sim 0.4$ at $De = 62$ ($\dot{\gamma} \simeq 1700$ s^{-1}). We experimentally verified that about 70% of the measured distances falls between $s^* = 3.5$ and $s^* = 5$ both for $De = 31$ and $De = 62$ (right panel of Figure 1c, Videos S1 and S2), with a throughput (particle concentration$\times$volumetric flow rate) of $\sim$1200 particles/s ($De = 31$) and $\sim$2400 particles/s ($De = 62$).

In the case of inertial ordering the distance between the particles depends on the particle Reynolds number $Re_\mathrm{p} = Re\,\beta^2$, where $Re = \rho Q/\eta H$ is the Reynolds number with ρ the fluid density, and $\beta = d/H$ is the confinement ratio [7]. Kahkeshani *et al.* [38] observed an average spacing $s^* = 5$ for $Re_p = 2.8$ and $s^* = 2.5$ for $Re_\mathrm{p} = 8.3$. In our experiments, however, we do not observe any Reynolds-dependent spacing; notice that our highest particle Reynolds number is $Re_\mathrm{p} = 0.0027$ (at $De = 62$), thus inertial effects are always negligible.

As stated above, particle ordering stems from hydrodynamic interactions that become relevant when the particles are sufficiently close to each other [7, 15, 29, 39]. Hence, particle concentration is an important parame-

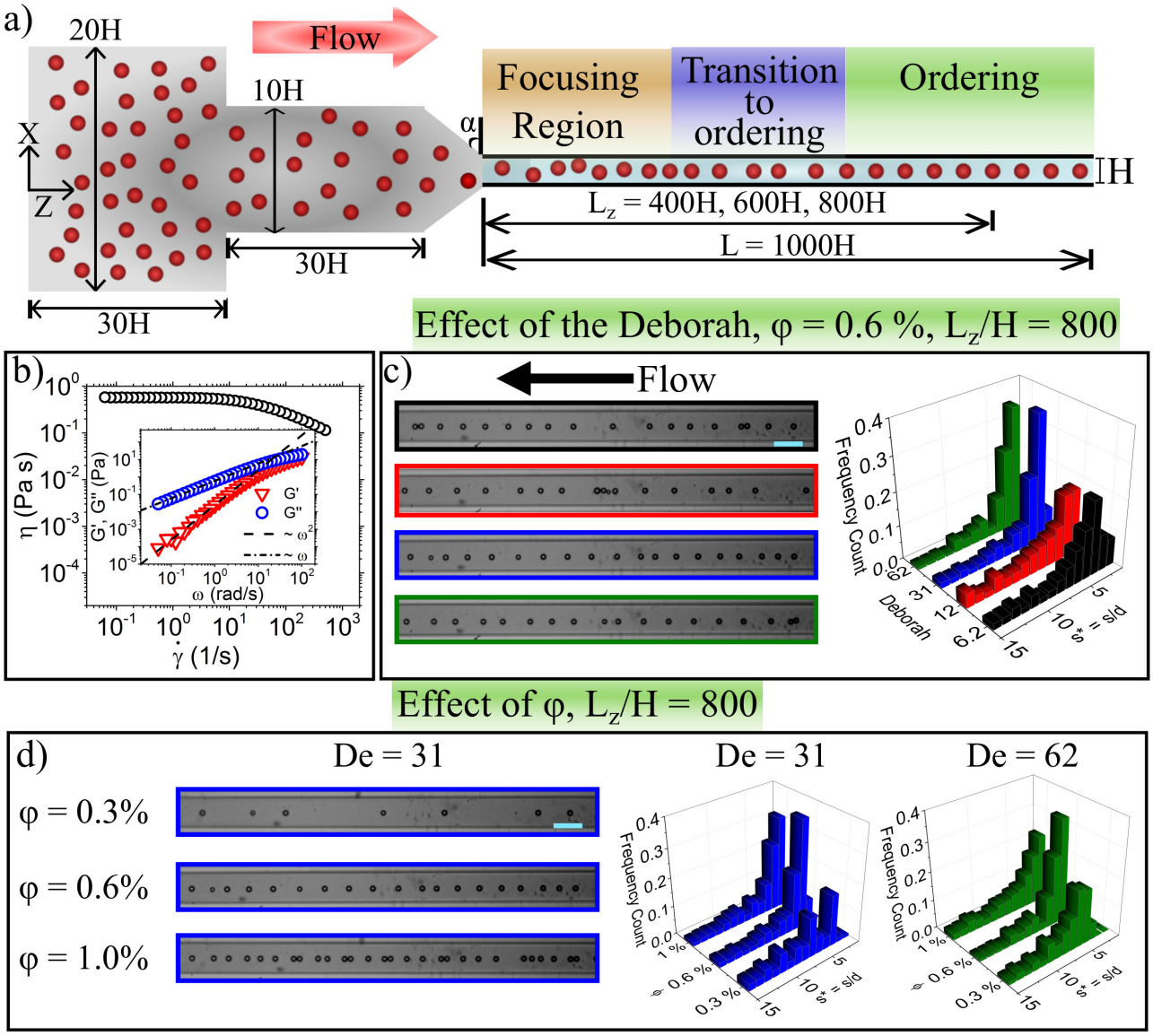

FIG. 1. **Fluid viscoelasticity drives self-assembly of particle trains in straight microfluidic channel** a) Schematic of the employed device with relevant dimensions. Particles converge gently to the glass channel, align after a certain length, and then self-order. The channel side is $H = 100$ μm, and the angle is $\alpha = 70°$. Dimensions are not to scale. The device in grey is a multi-contraction inlet made of polymethylmethacrylate. Such design prevents particle clogging at the entrance of the glass microchannel (light blue rectangle). b) Shear viscosity η as a function of the shear rate $\dot{\gamma}$ for hyaluronic acid (HA) at 1 wt% in PBS. The fluid displays a clear shear-thinning behavior above $\dot{\gamma} \sim 10$ s^{-1}. The inset shows the elastic modulus G' and the viscous modulus G'' as a function of the angular frequency ω for an imposed deformation $\gamma = 5\%$. The longest relaxation time $\lambda = 37$ ms is evaluated as the intersection between the dashed and the dash-dotted lines, identified as the so-called *terminal-region* [35]. c) Higher Deborah numbers $De = \lambda Q/H^3$ (Q is the volumetric flow rate) enhances the fraction of particles ordered at $s/d \sim 3.5$, where $d = 20$ μm is the particle diameter. Experimental snapshots at different De are also shown (same colour code of the histograms). Flow is from right to left. Volumetric particle fraction is $\phi = 0.6\%$. d) Particle ordering occurs at volumetric particle concentrations $\phi > 0.3\%$. At $\phi = 1\%$, an increasing number of "doublets" of particles is observed. Scale bar is 100 μm.

ter for the ordering mechanism. We then evaluated the spacing s^* at $L_z/H = 800$ as a function of the volumetric particle concentration ϕ for $De = 31$ and $De = 62$ (Figure 1d). At $\phi = 0.3$ vol%, the interparticle distances were quite large and random, and no clear ordering could be detected (top snapshot in Figure 1d), suggesting that hydrodynamic interactions in such conditions are weak. At $\phi = 0.6$ vol% the highest ordering efficiency was found for both $De = 31$ and $De = 62$ (Figure 1d). By further increasing the particle concentration to $\phi = 1$ vol% (bottom snapshot of Figure 1d, Video S3), we observed sequences of equally-spaced particles with some occasional

"doublets" or (less frequently) "triplets" of particles. Note that doublets of particles were not observed in the inertial ordering by Kahkeshani *et al.* [38]. Insights on the occurrence of doublets in viscoelastic self-assembly will be discussed below.

Particle trains are not observed in a near-constant viscosity liquid

To test the effect of the shear thinning on particle ordering, we carried out the same experiments for a hyaluronic acid solution 0.1 wt% in PBS with the addition of 25 wt% of glycerol to prevent particle sedimentation. Different from the HA 1 wt% used previously, the HA 0.1 wt% has a constant shear viscosity η in the whole range of shear rate $\dot{\gamma}$ investigated (Figure 2a). The relaxation time evaluated from the intersection of the dashed and the dashed dotted lines fitting the data at low frequencies (inset of Figure 2a) is $\lambda = 32$ ms, which is very similar to the relaxation time of the HA 1 wt%.

At $L_z/H = 800$, despite varying both Deborah numbers ($De = 26$ and $De = 52$) and particle concentration ($\phi = 0.3$ vol%, $\phi = 0.6$ vol%, and $\phi = 1$ vol%), we did not observe particle ordering (Figure 2(b-c)). Interestingly, we noticed the presence of sporadic "strings" of several very close particles, with few isolated particles between them, at both $\phi = 0.6$ vol% and $\phi = 1$ vol% (experimental snapshots shown in Figure 2c). Such strings were not observed for particles suspended in HA 1 wt%, where only doublets of particles were found mainly at $\phi = 1$ vol%. We also found that the number of particles strings in HA 0.1 wt% increased at $\phi = 1.5$ vol% (Video S4 for $De = 31$ and Video S5 for $De = 62$). The formation of these strings can be again ascribed to the existence of critical interparticle distance discussed above. D'Avino *et al.* [29] reported that the value of such distance increases as the *amount* of shear-thinning decreases, i.e., particle attraction is enhanced in a near constant-viscosity liquid, corroborating our experimental evidence. Finally notice that inertial effects are also expected to be negligible in this case, as the highest particle Reynolds number is $Re_p = 0.03$ (at $De = 62$).

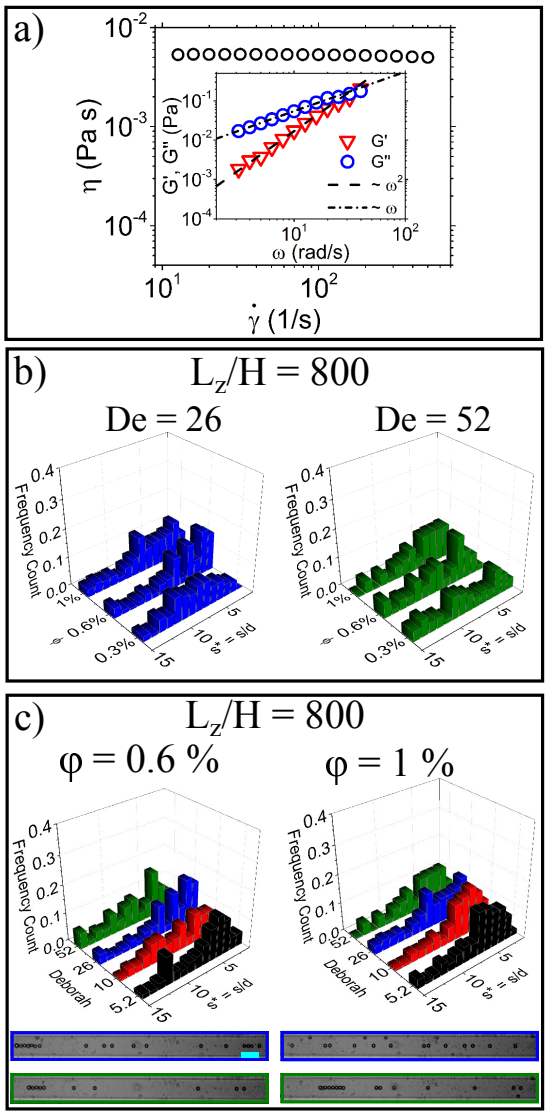

FIG. 2. **Particle trains are not observed in a near-constant viscosity liquid.** a) Shear viscosity η as a function of the shear rate $\dot{\gamma}$ for hyaluronic acid (HA) at 0.1 wt% in PBS with the addition of 25 wt% of Glycerol. The fluid is near-constant viscosity in the whole range of shear rates $\dot{\gamma}$ investigated. The inset shows the elastic modulus G' and the viscous modulus G'' as a function of the angular frequency ω for an imposed deformation $\gamma = 5\%$. The longest relaxation time $\lambda = 32$ ms is evaluated as the intersection between the dashed and the dash-dotted lines (who identify the so called *terminal-region* [35]). b) Effect of particle concentration ϕ on the normalized distance between the particles $s^* = s/d$ at two different Deborah numbers $De = 26$ and $De = 52$. Particle ordering is not observed in any of the conditions reported. c) Deborah number $De = \lambda Q/H^3$ (Q is the volumetric flow rate) does not affect significantly the distance between the particles s^*, at two different volume concentrations $\phi = 0.6\%$ and $\phi = 1\%$. Scale bar is 100 μm.

Numerical simulations

We investigated the particle ordering mechanism through numerical simulations (Figure 3) by considering that all the particles are aligned along the centerline when entering the channel [40–48].) We faced three main difficulties: the large number of particles of the experiments could not be dealt with in simulations, the imposed $De-$values were out of reach of computations (because of numerical instabilities), and the experimental confinement ratio $\beta = 0.2$ sould not be simulated because the relative velocities between the particles turned out to be very small and comparable with the numerical accuracy.

The first issue was tackled in the following way. Direct numerical simulations were used to calculate the relative velocities of a three-particle system for several initial interparticle distances. The selected distances between the particles and the corresponding computed interparticle

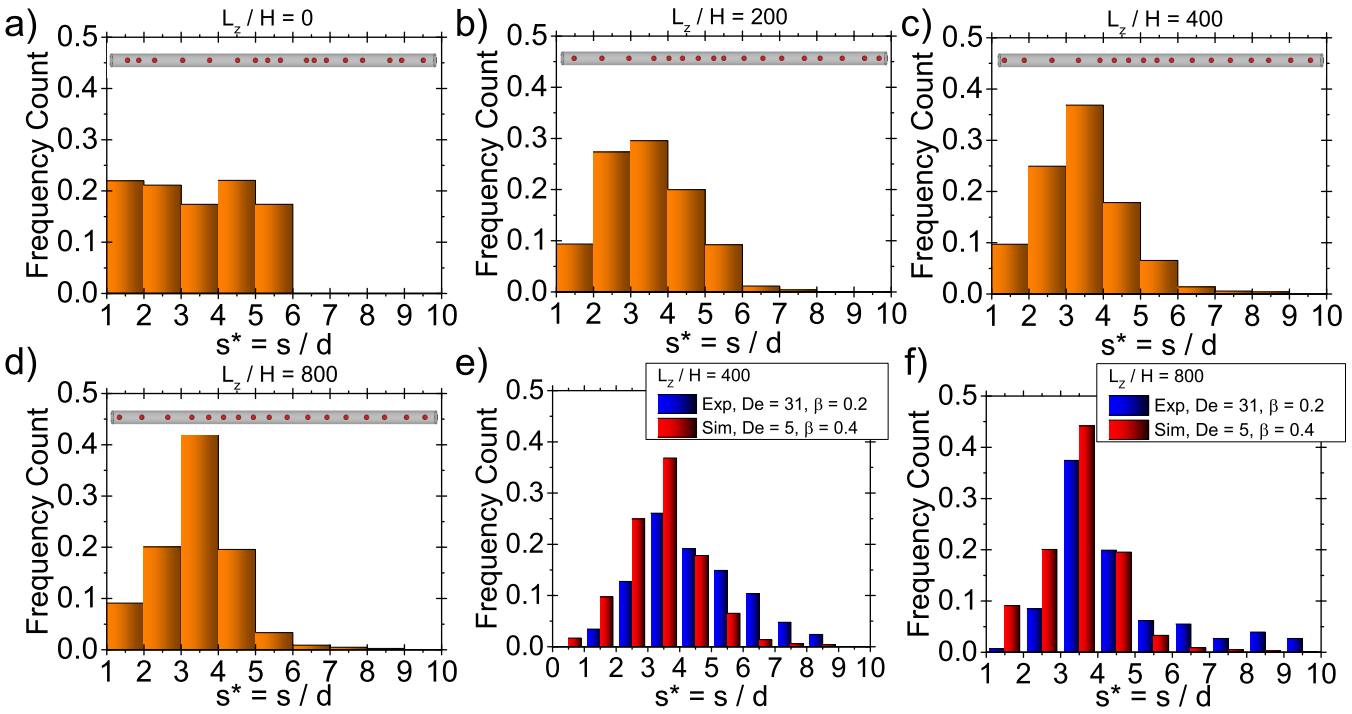

FIG. 3. **Numerical simulation are in good agreement with experiments** (a)-(d) Normalized distances between particles s^* at several distances from the channel inlet L_z/H. Screenshots from simulations are included as inset in each panel (full videos are available as Videos S6-S10). Particles at $L_z/H = 0$ are already aligned at the channel inlet. (e)-(f) Comparison between experimental and numerical distributions of s/d at $L_z/H = 400$ (e) and $L_z/H = 800$ (f). The experimental distributions are evaluated at $De = 31$ and $\beta = 0.2$, while the numerical simulations are carried out at $De = 5$ and $\beta = 0.4$ (see main text for more details on the choice of the parameter values in the simulations).

velocities were then used to model the multi-particle system, with the assumption that each particle in the train hydrodynamically interacted only with its trailing and leading spheres. In this way, the particle train dynamics could be computed by solving a simple set of ordinary differential equations [40]). The direct numerical simulations of the three-particle system was performed by choosing a two-mode Giesekus constitutive equation that accurately matched the HA 1 wt% in PBS rheology [40]).

The second and third issues were in fact solved together by noting that, as reported in D'Avino *et al.* [29] for a system of two particles suspended in Giesekus fluid, the relative particle velocity scaled as $\sim De\,\beta^3$. Based on this scaling, we simulated at $De = 5$ and $\beta = 0.4$, to describe the experimental situation with $De = 32$ and $\beta = 0.2$. The predicted dimensionless interparticle distances s^* at several distances from the inlet L_z/H are reported in Figure 3.

Comparison of simulations prediction with experiments

We first evaluated numerically the distributions of the interparticle distances at increasing distances from the channel inlet (Figures 3a-e). At $L_z/H = 0$ (channel inlet), particles were uniformly distributed within the range $1 < s^* < 6$ (Figure 3a and Video S6). As L_z/H increased, a clear peak at $s^* = 3.5$ was observed, in good agreement with experiments (Figure 3c-d and Videos S9 and S10). The comparison between the numerical distributions at increasing distances L_z/H also shows that the ordering dynamics is quite fast near to the entrance, but slows down at long distances from the inlet (the distribution at $L_z/H = 400$ looks very similar to that at $L_z/H = 800$).

It should again be remarked that the experiments show the general tendency to assemble trains of particles, but also show the presence of paired particles in doublets, intercalating ordered strings. This is more frequent as the particle loading increases (see Figure 1d). A similar trend is clearly visible also in the simulations (Videos S6-S10) thus confirming the qualitative good agreement between numerics and experiments.

We also compared the numerical distributions of s^* with the experimental ones, both at $L_z/H = 400$ and $L_z/H = 800$ (red and blue bars in Figure 3e-3f, respectively). The simulations slightly overestimate the peak as compared to experiments, especially at $L_z/H = 400$. This is not surprising as in the numerical simulations the particles enter the channel pre-aligned in contrast with the experimental conditions (random distribution over the channel inlet cross-section). However, a good qualitative agreement between the two distributions is observed, suggesting that the scaling with De and β proposed in D'Avino et al. [29] is reasonable. Taken together, these results show that the confinement ratio β, the Deborah number De and the channel length L_z provide some free-

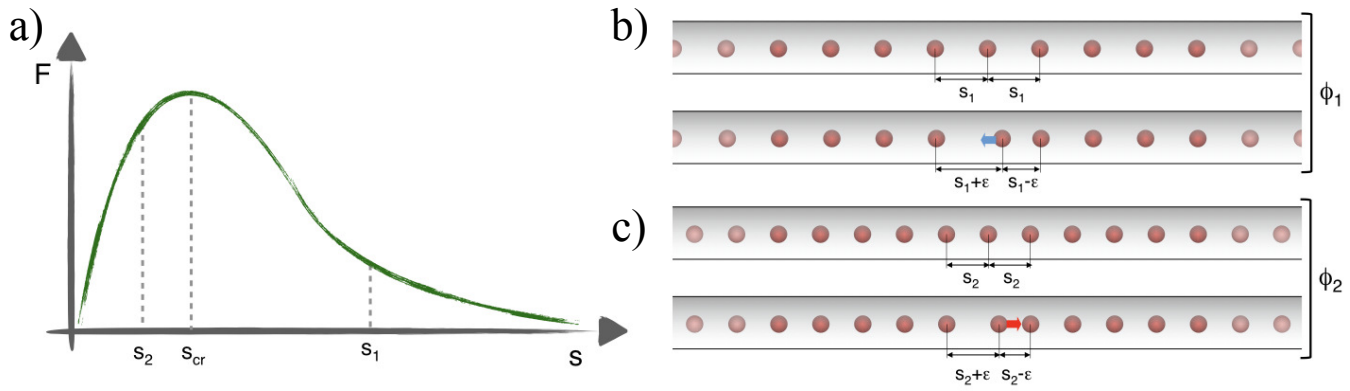

FIG. 4. **A stability analysis based on pairwise interactions supports the experimental and numerical results.** a) Sketch of the effective repulsive force between two particles in a viscoelastic fluid (see text) for a sufficiently high Deborah number. b) A train of equally spaced particles has been formed at some volume fraction ϕ_1 corresponding to a distance $s_1 > s_{\rm cr}$. A particle of the train displaced by a small amount ϵ experiences two different repulsive forces from the trailing (at distance $s_1+\epsilon$) and the leading (at distance $s_1-\epsilon$) sphere. Since s_1 is in the branch where the force $F(s)$ has a negative slope, the force between the displaced particle and the leading one is lower than the force between the particle and the trailing sphere. The net force is, then, towards the trailing sphere (blue arrow) and the interparticle distances are restored to the original value s_1. c) The same scenario as in panel b) where the volume fraction is $\phi_2 > \phi_1$ and the interparticle distance is $s_2 < s_{\rm cr}$. Now, the force between the displaced sphere and the leading one is higher than the force between the particle and the trailing sphere. Thus, the displaced sphere moves towards the leading one and a pair is formed.

dom of tuning to achieve particle ordering in different flow conditions. As a final note, we also tried to perform experiments at $\beta = 0.4$. In this case, however, we observed significant clogging within the glass channel.

Viscoelasticity-induced effective repulsive force leads to ordering or pairing in particle trains

A simple qualitative argument can be used to justify the observed formation of trains of equally-spaced particles in confined viscoelastic flows. We start from the assumption that the particles move 'caged' at the channel centerline by the normal stresses arising in a viscoelastic flow [23]. We then examine the stability of the train arrangement, by slightly perturbing its *1D* crystal-like configuration. To keep the analysis simple, we also assume that a generic particle in the train interacts (hydrodynamically) with only the two nearest neighbors. As shown in Figure 7 of Ref. [29], for De larger than some critical value $De_{\rm cr}$ (its exact value depending on confinement ratio and fluid rheology), two particles display a velocity difference which makes them to separate from each other, as if they were subjected to a repulsion force $F(s)$. This repulsive force $F(s)$ at large $De-$values (as in our experiments) is non-monotonic, and presents a maximum at a critical inter-particle distance $s_{\rm cr}$. A qualitative sketch of the force versus distance curve is depicted in Figure 4a, which is drawn by analogy with the results of direct numerical simulations reported in Ref. [29] for a relatively high value of the Deborah number. A simple stability argument gives the following conclusions. If the train spacing is larger than $s_{\rm cr}$, say s_1, a local small perturbation ϵ of the position of a particle generates an asymmetric spacing around that particle, triggering a dynamics that drives the train to recover its original spacing s_1. Indeed, the repulsion between slightly closer particles at $s_1 - \epsilon$ is stronger than that between the more distant ones at $s_1 + \epsilon$ (see Figure 4b and caption therein). On the contrary, if the train spacing is smaller than $s_{\rm cr}$, say s_2, the reverse dynamics occurs, whereby the closer particles will tend to come into contact, forming a doublet (Figure 4c)). Thus, a train with a large spacing (with respect to $s_{\rm cr}$) is stable, whereas a train with a small spacing is unstable, and might develop particle pairing. Particle ordering and particle pairing naturally stem from the stability analysis.

The dimensionless train spacing s^* is of course linked to the actual volume fraction used in the experiments, by the purely geometrical relation [40]:

$$s^*\phi = \phi_{\rm mp}\beta^2, \tag{2}$$

where $\phi_{\rm mp}$ is the maximum packing with spherical particles inscribed in the channel. In the case of a square channel, $\phi_{\rm mp} = \pi/6$. Thus, large train spacings, i.e., volume fractions smaller than $\phi_{\rm cr} = \phi_{\rm mp}\beta^2/s^*_{\rm cr}$, promote particle trains ('ordering'), whereas small spacings induce particle 'pairing' within the train. Notice that, as mentioned above, Eq. 2 is derived by geometrical considerations. Hence, the train spacing s^* does not depend on the fluid rheology. On the other hand, the shape of the force vs. particle distance curve in Figure 4a as well as the critical value $s^*_{\rm cr}$ are affected by the rheological properties of the suspending fluid. For instance, at lower Deborah numbers, the force becomes attractive at small interparticle distances [29], promoting doublets formation. Higher viscosities of a Newtonian solvent move $s^*_{\rm cr}$ towards lower values, although the force magnitude is reduced [29], delaying the ordering dynamics. However, a

systematic investigation of the effect of fluid rheology on the shape of the pair-wise force as well as the physical arguments leading to such force are still lacking, which will be part of the future work.

The results of this simple analysis do correspond to both our experimental observations and numerical predictions. In view of this agreement, we can conclude that viscoelasticity enters the train stability scenario only through the 'shape' of the repulsive pairwise force, and modulates the kinetics of train formation, when it occurs. Furthermore, the experimentally observed importance of the shear-thinning behaviour of the viscoelastic liquid is confirmed within this heuristic analysis, as the $De > De_{\rm cr}$ condition, giving the qualitative force-spacing scenario of Figure 4a, corresponds to shear-thinning conditions.

In light of the simple stability analysis, particle pairing can be drastically reduced by employing particle concentrations lower than $\phi_{\rm cr}$. This is very important for applications in flow cytometry and encapsulation where particle or cell pairing is detrimental. We also anticipate that fluids with different elastic properties will lead to a different shape of the repulsive force curve, providing additional degree of freedom to prevent particle/cell pairing.

CONCLUSIONS AND PERSPECTIVES

In this work, we discover that fluid viscoelasticity drives self-assembly of particle trains along the centerline of a straight microfluidic channel. In our experiments, particles with diameter $d = 20$ μm first align at the channel centreline of a square-shaped glass microchannel with height $H = 100$ μm, and then self-order, forming trains with a throughput up-to 2400 particle/second. Particle trains in viscoelastic liquids are thus easily formed, without the need of designing complex microfluidic platforms or of using external control systems.

Our results show that shear-thinning of the suspending liquid is required to achieve the ordering. We find good qualitative agreement between experiments and numerical simulations. We also find that the predominant distance between ordered particles does not depend on the Deborah number De nor on the distance from the inlet $L_{\rm z}/H$. On the other hand, an increase of De and $L_{\rm z}/H$ enhances the fraction of ordered particles. As loading increases, particle ordering is somehow perturbed by the formation of particle pairs.

Experimental and numerical evidences can be justified by a simple stability analysis, based on the presence of an effective peculiar repulsive potential between particles. In channel flows, such 'repulsive field', that stems from hydrodynamic interactions in viscoelastic liquids at large De, promotes either 'particle ordering' or 'particle pairing'. This picture is indeed very intriguing and might be of larger generality: as in other situations [49, 50], self-assembly can come out from repulsion in geometrically constrained situations, like our *1D* caging at the channel centreline. From the same stability argument, we learn that particle pairing, which is detrimental in applications related to flow cytometry and encapsulation, can be avoided by tuning the fluid rheology and particle concentration. Therefore, testing the effect of different viscoelastic shear-thinning liquids and particle concentrations on the train formation is worth of investigation.

The present results can be applied to biomedical engineering and material science. For instance, ordering of biological objects at the channel centerline would be beneficial for optimised flow cytometry [1, 3] and deterministic cell encapsulation [5, 6]. In high throughput flow cytometry, for instance, ordering may prevent cells from overlapping at large cell loadings, which wascommonly observed in elastic constant-viscosity liquids (Figure 2c). A constant spacing between particles is also beneficial for the real-time analysis of flowing cells since it reduces computational costs associated with data analysis [18]. Shear-thinning fluids display an almost flat velocity profile near the channel centerline at $De > 1$, thus flowing cells would potentially be undeformed (or only slightly deformed), which is optimal for manipulation of delicate cells [32]. Furthermore, as compared to inertial microfluidics, the relatively low flow rates needed to achieve ordering are more compatible with downstream droplet generation systems. In material science, our results will prompt further efforts towards microfluidic fabrication of novel materials to enhance localised properties at micrometer-size level [51–54]. Novel techniques such as the 'Stokes Trap' [55] can be employed to further understand hydrodynamic particle-particle interactions in viscoelastic liquids.

ACKNOWLEDGEMENTS

F.D.G. and A.Q.S. gratefully acknowledge the support of the Okinawa Institute of Science and Technology Graduate University with subsidy funding from the Cabinet Office, Government of Japan. A.Q.S. also acknowledges funding from the Japan Society for the Promotion of Science (Grants-in-Aid for Scientific Research (B), Grant No. 18H01135). and Grants-in-Aid for Scientific Research (C), Grant No. 17K06173).

[1] John Oakey, Robert W Applegate Jr, Erik Arellano, Dino Di Carlo, Steven W Graves, and Mehmet Toner, "Particle focusing in staged inertial microfluidic devices for flow cytometry," Analytical chemistry **82**, 3862–3867 (2010).

[2] David Erickson and Dongqing Li, "Integrated microfluidic devices," Analytica chimica acta **507**, 11–26 (2004).

[3] Soojung Claire Hur, Henry Tat Kwong Tse, and Dino Di Carlo, "Sheathless inertial cell ordering for extreme throughput flow cytometry," Lab on a Chip **10**, 274–280 (2010).

[4] Daniel R Gossett, Westbrook M Weaver, Albert J Mach, Soojung Claire Hur, Henry Tat Kwong Tse, Wonhee Lee, Hamed Amini, and Dino Di Carlo, "Label-free cell separation and sorting in microfluidic systems," Analytical and bioanalytical chemistry **397**, 3249–3267 (2010).

[5] Jon F Edd, Dino Di Carlo, Katherine J Humphry, Sarah Köster, Daniel Irimia, David A Weitz, and Mehmet Toner, "Controlled encapsulation of single-cells into monodisperse picolitre drops," Lab on a Chip **8**, 1262–1264 (2008).

[6] Evelien WM Kemna, Rogier M Schoeman, Floor Wolbers, Istvan Vermes, David A Weitz, and Albert Van Den Berg, "High-yield cell ordering and deterministic cell-in-droplet encapsulation using dean flow in a curved microchannel," Lab on a Chip **12**, 2881–2887 (2012).

[7] Wonhee Lee, Hamed Amini, Howard A Stone, and Dino Di Carlo, "Dynamic self-assembly and control of microfluidic particle crystals," Proceedings of the National Academy of Sciences **107**, 22413–22418 (2010).

[8] James E Hallett, Francesco Turci, and C Patrick Royall, "Local structure in deeply supercooled liquids exhibits growing lengthscales and dynamical correlations," Nature communications **9**, 3272 (2018).

[9] JL Aragones, JP Steimel, and A Alexander-Katz, "Elasticity-induced force reversal between active spinning particles in dense passive media," Nature communications **7**, 11325 (2016).

[10] Kevin A Arpin, Agustin Mihi, Harley T Johnson, Alfred J Baca, John A Rogers, Jennifer A Lewis, and Paul V Braun, "Multidimensional architectures for functional optical devices," Advanced Materials **22**, 1084–1101 (2010).

[11] Pai Wang, Filippo Casadei, Sicong Shan, James C Weaver, and Katia Bertoldi, "Harnessing buckling to design tunable locally resonant acoustic metamaterials," Physical Review Letters **113**, 014301 (2014).

[12] Scott J Hollister, "Porous scaffold design for tissue engineering," Nature materials **4**, 518–524 (2005).

[13] Paul Calvert, "Printing cells," Science **318**, 208–209 (2007).

[14] G Segre and AJ Silberberg, "Behaviour of macroscopic rigid spheres in poiseuille flow part 2. experimental results and interpretation," Journal of fluid mechanics **14**, 136–157 (1962).

[15] Jean-Philippe Matas, Virginie Glezer, Élisabeth Guazzelli, and Jeffrey F Morris, "Trains of particles in finite-reynolds-number pipe flow," Physics of Fluids **16**, 4192–4195 (2004).

[16] Dino Di Carlo, Daniel Irimia, Ronald G Tompkins, and Mehmet Toner, "Continuous inertial focusing, ordering, and separation of particles in microchannels," Proceedings of the National Academy of Sciences **104**, 18892–18897 (2007).

[17] J-A Kim, J Lee, C Wu, S Nam, D Di Carlo, and Wonhee Lee, "Inertial focusing in non-rectangular cross-section microchannels and manipulation of accessible focusing positions," Lab on a Chip **16**, 992–1001 (2016).

[18] Keisuke Goda, Ali Ayazi, Daniel R Gossett, Jagannath Sadasivam, Cejo K Lonappan, Elodie Sollier, Ali M Fard, Soojung Claire Hur, Jost Adam, Coleman Murray, *et al.*, "High-throughput single-microparticle imaging flow analyzer," Proceedings of the National Academy of Sciences **109**, 11630–11635 (2012).

[19] Gaetano D'Avino, Giovanni Romeo, Massimiliano M Villone, Francesco Greco, Paolo A Netti, and Pier Luca Maffettone, "Single line particle focusing induced by viscoelasticity of the suspending liquid: theory, experiments and simulations to design a micropipe flow-focuser," Lab on a Chip **12**, 1638–1645 (2012).

[20] Seungyoung Yang, Jae Young Kim, Seong Jae Lee, Sung Sik Lee, and Ju Min Kim, "Sheathless elasto-inertial particle focusing and continuous separation in a straight rectangular microchannel," Lab on a Chip **11**, 266–273 (2011).

[21] Ilaria De Santo, Gaetano D'Avino, Giovanni Romeo, Francesco Greco, Paolo A Netti, and Pier Luca Maffettone, "Microfluidic lagrangian trap for brownian particles: Three-dimensional focusing down to the nanoscale," Physical Review Applied **2**, 064001 (2014).

[22] AM Leshansky, A Bransky, N Korin, and U Dinnar, "Tunable nonlinear viscoelastic "focusing" in a microfluidic device," Physical Review Letters **98**, 234501 (2007).

[23] Gaetano D'Avino, Francesco Greco, and Pier Luca Maffettone, "Particle migration due to viscoelasticity of the suspending liquid and its relevance in microfluidic devices," Annual Review of Fluid Mechanics **49**, 341–360 (2017).

[24] Xinyu Lu, Chao Liu, Guoqing Hu, and Xiangchun Xuan, "Particle manipulations in non-newtonian microfluidics: A review," Journal of Colloid and Interface Science (2017).

[25] Dan Yuan, Qianbin Zhao, Sheng Yan, Shi-Yang Tang, Gursel Alici, Jun Zhang, and Weihua Li, "Recent progress of particle migration in viscoelastic fluids," Lab on a Chip **18**, 551–567 (2018).

[26] Nan Xiang, Xinjie Zhang, Qing Dai, Jie Cheng, Ke Chen, and Zhonghua Ni, "Fundamentals of elasto-inertial particle focusing in curved microfluidic channels," Lab on a Chip **16**, 2626–2635 (2016).

[27] Nan Xiang, Zhonghua Ni, and Hong Yi, "Concentration-controlled particle focusing in spiral elasto-inertial microfluidic devices," Electrophoresis **39**, 417–424 (2018).

[28] Ah Reum Kang, Sung Won Ahn, Seong Jae Lee, Byunghwan Lee, Sung Sik Lee, and Ju Min Kim, "Medium viscoelastic effect on particle segregation in concentrated suspensions under rectangular microchannel flows," Korea-Australia Rheology Journal **23**, 247–254 (2011).

[29] G. D'Avino, M. A. Hulsen, and P. L. Maffettone, "Dynamics of pairs and triplets of particles in a viscoelastic fluid flowing in a cylindrical channel," Comput. Fluids **86**, 45–55 (2013).

[30] Francesco Del Giudice, Gaetano D'Avino, Francesco Greco, Paolo A Netti, and Pier Luca Maffettone, "Effect of fluid rheology on particle migration in a square-shaped microchannel," Microfluidics and Nanofluidics **19**, 95–104 (2015).

[31] Di Li and Xiangchun Xuan, "Fluid rheological effects on particle migration in a straight rectangular microchannel," Microfluidics and Nanofluidics **22**, 49 (2018).

[32] Francesco Del Giudice, Shivani Sathish, Gaetano D'Avino, and Amy Q Shen, ""from the edge to the center": viscoelastic migration of particles and cells in a strongly shear-thinning liquid flowing in a microchannel," Analytical Chemistry **89**, 13146–13159 (2017).

[33] David J Guckenberger, Theodorus E de Groot, Alwin MD Wan, David J Beebe, and Edmond WK Young, "Micromilling: a method for ultra-rapid prototyping of plastic microfluidic devices," Lab on a Chip **15**, 2364–2378 (2015).

[34] John C Crocker and David G Grier, "Methods of digital video microscopy for colloidal studies," Journal of colloid and interface science **179**, 298–310 (1996).

[35] Christopher W Macosko and Ronald G Larson, *Rheology: principles, measurements, and applications* (VCH New York, 1994).

[36] Francesco Del Giudice, Francesco Greco, Paolo Antonio Netti, and Pier Luca Maffettone, "Is microrheometry affected by channel deformation?" Biomicrofluidics **10**, 043501 (2016).

[37] G D'Avino and PL Maffettone, "Particle dynamics in viscoelastic liquids," Journal of Non-Newtonian Fluid Mechanics **215**, 80–104 (2015).

[38] Soroush Kahkeshani, Hamed Haddadi, and Dino Di Carlo, "Preferred interparticle spacings in trains of particles in inertial microchannel flows," Journal of Fluid Mechanics **786** (2016).

[39] Katherine J Humphry, Pandurang M Kulkarni, David A Weitz, Jeffrey F Morris, and Howard A Stone, "Axial and lateral particle ordering in finite reynolds number channel flows," Physics of Fluids **22**, 081703 (2010).

[40] See supplemental material at [url will be inserted by publisher] for details on the injection policy, more details on the adopted procedure, the validity of the assumptions and the validation. The full derivation of Eq. 2 is also reported.

[41] Ronald G Larson, *Constitutive Equations for Polymer Melts and Solutions* (Butterworth-Heinemann, 2013).

[42] Arjen CB Bogaerds, Anne M Grillet, Gerrit WM Peters, and Frank PT Baaijens, "Stability analysis of polymer shear flows using the extended pom–pom constitutive equations," J. non-Newtonian Fluid Mech. **108**, 187–208 (2002).

[43] Robert Guénette and Michel Fortin, "A new mixed finite element method for computing viscoelastic flows," J. non-Newtonian Fluid Mech. **60**, 27–52 (1995).

[44] Alexander N Brooks and Thomas JR Hughes, "Streamline upwind/petrov-galerkin formulations for convection dominated flows with particular emphasis on the incompressible navier-stokes equations," Comput. Methods Appl. Mech. Eng. **32**, 199–259 (1982).

[45] Raanan Fattal and Raz Kupferman, "Constitutive laws for the matrix-logarithm of the conformation tensor," J. non-Newtonian Fluid Mech. **123**, 281–285 (2004).

[46] Martien A Hulsen, Raanan Fattal, and Raz Kupferman, "Flow of viscoelastic fluids past a cylinder at high weissenberg number: stabilized simulations using matrix logarithms," J. non-Newtonian Fluid Mech. **127**, 27–39 (2005).

[47] Howard H Hu, Neelesh A Patankar, and MY Zhu, "Direct numerical simulations of fluid–solid systems using the arbitrary lagrangian–eulerian technique," J. Comput. Phys. **169**, 427–462 (2001).

[48] Arjen CB Bogaerds, Martien A Hulsen, Gerrit WM Peters, and Frank PT Baaijens, "Stability analysis of injection molding flows," J. Rheology **48**, 765–785 (2004).

[49] P Pieranski, "Two-dimensional interfacial colloidal crystals," Physical Review Letters **45**, 569–572 (1980).

[50] DG Lee, P Cicuta, and D Vella, "Self-assembly of repulsive interfacial particles via collective sinking," Soft Matter **13**, 212–221 (2017).

[51] Kevin S Paulsen, Dino Di Carlo, and Aram J Chung, "Optofluidic fabrication for 3d-shaped particles," Nature communications **6** (2015).

[52] Bing Xu, Yang Shi, Zhao-Xin Lao, Jin-Cheng Ni, Guoqiang Li, Yanlei Hu, Jiawen Li, Jia-ru Chu, Dong Wu, and Koji Sugioka, "Real-time two-photon-lithography in controlled flow to create a single-microparticle-array and particle-cluster-array for optofluidic imaging," Lab on a Chip (2017).

[53] Qibin Zhao, Chris E Finlayson, David RE Snoswell, Andrew Haines, Christian Schäfer, Peter Spahn, Goetz P Hellmann, Andrei V Petukhov, Lars Herrmann, Pierre Burdet, *et al.*, "Large-scale ordering of nanoparticles using viscoelastic shear processing," Nature communications **7**, ncomms11661 (2016).

[54] Sagar Yadavali, Heon-Ho Jeong, Daeyeon Lee, and David Issadore, "Silicon and glass very large scale microfluidic droplet integration for terascale generation of polymer microparticles," Nature communications **9**, 1222 (2018).

[55] Anish Shenoy, Christopher V Rao, and Charles M Schroeder, "Stokes trap for multiplexed particle manipulation and assembly using fluidics," Proceedings of the National Academy of Sciences , 201525162 (2016).